Published in final edited form as:
J Mater Sci Mater Med. 2013 February ; 24(2): 343–354. doi:10.1007/s10856-012-4793-1.

Nanoparticles of cobalt-substituted hydroxyapatite in regeneration of mandibular osteoporotic bones

Nenad Ignjatović[1], **Zorica Ajduković**[2], **Vojin Savić**[3], **Stevo Najman**[3], **Dragan Mihailović**[4], **Perica Vasiljević**[5], **Zoran Stojanović**[1], **Vuk Uskoković**[6], and **Dragan Uskoković**[1]

[1]Institute of Technical Sciences, Serbian Academy of Sciences and Arts, Belgrade, Serbia

[2]Department of Prosthodontics, Clinic of Stomatology, Faculty of Medicine, University of Niš, Niš, Serbia

[3]Institute of Biomedical Research, Faculty of Medicine, University of Niš, Niš, Serbia

[4]Institute of Pathology, Faculty of Medicine, University of Niš, Niš, Serbia

[5]Department of Biology and Ecology, Faculty of Science, University of Niš, Niš, Serbia

[6]Therapeutic Micro and Nanotechnology Laboratory, Department of Bioengineering and Therapeutic Sciences, University of California, San Francisco, USA

Abstract

Indications exist that paramagnetic calcium phosphates may be able to promote regeneration of bone faster than their regular, diamagnetic counterparts. In this study, analyzed was the influence of paramagnetic cobalt-substituted hydroxyapatite nanoparticles on osteoporotic alveolar bone regeneration in rats. Simultaneously, biocompatibility of the material was tested *in vitro*, on osteoblastic MC3T3-E1 and epithelial Caco-2 cells in culture. The material was shown to be biocompatible and nontoxic when added to epithelial monolayers *in vitro*, while it caused a substantial decrease in the cell viability as well as deformation of the cytoskeleton and cell morphology when incubated with the osteoblastic cells. In the course of six months after the implantation of the material containing different amounts of cobalt, ranging from 5 – 12 wt%, in the osteoporotic alveolar bone of the lower jaw, the following parameters were investigated: histopathological parameters, alkaline phosphatase and alveolar bone density. The best result in terms of osteoporotic bone tissue regeneration was observed for hydroxyapatite nanoparticles with the largest content of cobalt ions. The histological analysis showed a high level of reparatory ability of the nanoparticulate material implanted in the bone defect, paralleled by a corresponding increase in the alveolar bone density. The combined effect of growth factors from autologous plasma admixed to cobalt-substituted hydroxyapatite was furthermore shown to have a crucial effect on the augmented osteoporotic bone regeneration upon the implantation of the biomaterial investigated in this study.

Keywords

nanoparticles; hydroxyapatite; Ca/Co-HAp; osteoporosis; alveolar bone; regeneration

Introduction

Osteoporosis is a metabolic disease that affects millions of people around the globe. It is a progressive, systemic skeletal disease characterized by low bone density and micro-architectural bone damage, with the consecutive increase in bone fragility and susceptibility to fracture [1]. Osteoporosis of cancellous bone leads to thinning of trabeculae, widening of marrow and decreased bone density in the center of the bone, while in the cortical region

overall thinning occurs at the periphery [1–3]. One of the approaches for treating osteoporosis in oral and maxillofacial areas has involved implantation of different types of biomaterials [3–7]. The quest for materials performing better than those currently in use is, however, ongoing, with a special focus on nanoparticulate biomaterials.

A special attention in implantology and prosthetics is nowadays directed towards synthetic materials with the properties of natural bone, such as biomaterials composed of hydroxyapatite (HAp) [8, 9]. HAp is chemically similar to mineral components of bone and hard tissues in mammals, and is also bioconductive, that is, it supports bone growth and osseointegration. Reconstructions of mandibular bone defects using HAp have been in clinical practice for more than 20 years now [10]. Fillers based on HAp have also been used for the reconstruction of osteoporotic bone defects prior to fixation [11]. HAp in combination with bisphosphonates has also showed satisfactory results in the treatment and reconstruction of osteoporotic bone [12]. In addition, nanoparticulate HAp may have advantages over its microparticulate forms in terms of enabling greater osseointegration enhancement [13]. Osteoblast adhesion was thus shown to be stronger on compacts composed of nanoparticulate HAp than on those comprising microsized particles of the same chemical composition [14].

Physicochemical and biological properties of HAp can be amplified via modification of its composition and crystal structure [15]. Various elements have been used to dope HAp with in order to modify its properties [16, 17, 18]. Strontium-substituted HAp was synthesized as a potential material for the reconstruction of osteoporotic bone [19]. Reported were also *in vitro* studies on HAp systems combined with maghemite, showing significantly enhanced proliferation and differentiation of osteoblasts under static magnetic fields [20]. These results indicate that the magnetic field may be an important factor applicable in augmenting bone tissue regeneration and increasing the efficacy of the treatment of bone defects in bone tissue engineering [21].

Cobalt as a substitute in HAp was chosen because: (a) it has not been assessed yet as an ionic substitute for calcium in HAp applicable in reparation of hard tissues; (b) it has previously been shown as able to provide a finite magnetic moment in magnetic field to otherwise diamagnetic pure HAp, with saturation magnetizations reaching 10 emu/g at 5 K; and (c) it has been used as an element of alloys applied as surgical implants for years [22].

The research reported here aimed to investigate the influence of nanoparticulate HAp in whose crystal lattice Ca^{2+} ions were partially substituted with different amounts of Co^{2+} ions on the time scale required for the development of angiogenesis and regeneration of osteoporotic alveolar bone *in vivo*. Co^{2+} ions from the implanted Ca/Co-HAp nanomaterial were hypothesized to be able to act in synergy with aminopeptidase enzymes and boost proliferation and migration of the endothelial cells important for the process of osteogenesis. Each bone substitute that enhances osteogenesis may be useful in strengthening the weakened osteoporotic bone. Co-substituted HAp was examined in this study for its ability to act as one such osteogenic implant in reparation of osteoporotic jawbone. In order to improve angiogenesis, the effect of blood and blood plasma as catalyst components, admixed to Ca/Co-HAp, was investigated as well. Simultaneously, tests were conducted to assess biocompatibility of the given particles *in vitro*, and that on osteoblastic MC3T3-E1 and epithelial Caco-2 cells in culture.

Materials and methods

Powders of calcium hydroxyapatite (HAp) and calcium cobalt hydroxyapatite (Ca/Co-HAp), in which Ca ions are replaced with ~ 5% (HAp/Co1) and ~ 12% (HAp/Co2) of Co^{2+} ions,

were synthesized hydrothermally in a stainless steel reactor (Parr 4530 Floor Stand Pressure Reactor) at a temperature of 200 °C and constant mixing of 400 rpm during 8 h [23, 16]. The phase composition of the synthesized material was determined by means of X-ray diffraction (XRD; Philips PW1050 diffractometer with Cu $K\alpha_{1,2}$ Ni – filtered radiation). The size distribution of the particles was determined after intense sonication of dry and suspended powders by means of laser diffraction (LD) particle size analysis (Malvern Instruments Mastersizer 2000). Morphological characteristics were measured using field emission scanning electron microscopy (Carl Zeis FE SEM Suppra 35VP). Co content was confirmed using inductively coupled plasma (ICP) emission spectroscopy analysis (Thermo Scientific iCAP 6300 spectrometer) [16].

In vitro experimental design

Mouse calvarial preosteoblastic cell line, MC3T3-E1 subclone 4, and the human intestinal Caco-2 cell line were both purchased from American Tissue Culture Collection (*ATCC*, Rockville, MD). MC3T3-E1 cells were cultured in Alpha Minimum Essential Medium (α-MEM; *Gibco*) supplemented with 10% fetal bovine serum (FBS, *Invitrogen*) and no ascorbic acid (AA). Caco-2 cells were cultured in Eagle's Minimum Essential Medium with Earle's Balanced Salt Solution, 1 mM sodium pyruvate, 20% fetal bovine serum (Sigma), and 1% penicillin-streptomycin antibiotic solution. The medium was replaced every 48 h, and the cultures were incubated at 37 °C in a humidified atmosphere containing 5% CO_2. Every 7 days, the cells were detached from the surface of the 75 cm^2 cell culture flask (*Greiner Bio-One*) using 0.25 wt% trypsin, washed, centrifuged (1000 rpm × 3 min), resuspended in 10 ml of the cell culture medium and subcultured in 1:7 volume ratio. Cell passages 6 – 12 were used for the experiments reported hereby. The cultures were regularly examined under an optical microscope to monitor growth and possible contamination.

MC3T3-E1 cells were seeded on glass cover slips placed in 24 well plates and 500 μl of α-MEM supplemented with 10% fetal bovine serum (FBS, *Invitrogen*) and no AA at the density of 6×10^4 cells per well. After 5 days of incubation, nearly confluent cells were treated with α-MEM containing 50 μg/ml AA as the mineralization inductor. At the same time, 2 mg/cm^2 of particles were added to the cells and incubated for 7 days. Alpha-MEM supplemented with 50 μg/ml AA was replenished every 48 h. After the given period, one portion of cells was fixed for 15 min in 3.7 wt% paraformaldehyde at room temperature and then stained for f-actin and nucleus using phalloidin-tetramethylrhodamine (AlexaFluor 555, Invitrogen) and 4′,6-diamidino-2-phenylindole dihydrochloride nuclear counterstain (DAPI, Invitrogen), following a previously described protocol [24]. The cover slips containing the fixed and stained cells were mounted onto glass slides using hard set vectashield and nail hardener and were subsequently imaged on a confocal laser scanning microscope – C1si (UCSF Nikon Imaging Center) at 60 – 100 x magnification in oil. All the experiments were carried out in triplicates. The other portion of the cells was used for running an MTT (3-[4, 5-dimethylthiazol-2-yl]-2, 5-diphenyl tetrazolium bromide) *in vitro* toxicological assay. The test proceeded by adding 20 μl of 5 mg/ml MTT (*Sigma M-5655*) in PBS to each well already containing 200 μl of cell culture media. Following 2 h incubation at 37 °C, 220 μl of MTT solubilization solution (*Sigma M-5655*) were added to each well. The plate was shaken at room temperature for an hour and samples from each well were analyzed for absorbance at 570 nm on a UV/Vis spectrophotometric microplate reader (*Molecular Devices: Spectra Max 190*). All the particle types were analyzed in triplicates and the resulting absorbance values were normalized to the negative control.

Caco-2 cells were seeded at the density of 7.5×10^4 cells/well in 24 well plates and reached confluency in 5 – 7 days. To ensure that the cells were polarized at the onset of the experiment, the latter began only when the cells seeded in parallel in Transwells placed in

24 well plates at the same density of 7.5×10^4 cells/well reached trans-epithelial electrical resistance (TEER) values of > 1000 Ω. Confluent, polarized Caco-2 cells grown on glass slides in 24 well plates were treated with 2 mg/cm^2 of particles resuspended in 500 μl of the cell culture medium, and incubated for 4 h at 37 °C. After the given incubation period, the epithelial cells were fixed for 5 min in −20 °C methanol and then stained for zonula occludens-1 (ZO-1) and nucleus using rabbit anti-ZO-1 primary antibody (Zymed Lab), AlexaFluor 555 goat anti-rabbit IgG secondary antibody (Invitrogen), and 4′,6-diamidino-2-phenylindole dihydrochloride nuclear counterstain (DAPI, Invitrogen), respectively, following a previously described [24]. Cover slips containing the fixed and stained cells were mounted onto glass slides using vectashield and nail hardener and imaged in oil under a confocal laser scanning microscope – C1si (UCSF Nikon Imaging Center) at 60 – 100 x magnification. All the experiments were done in triplicates. Volume-rendered z-stack images (12 – 15 of them) spaced by 1 μm were collected at identical laser intensities and analyzed for the fluorescence intensity using ImageJ and NIS Elements software. The thickness of ZO-1 conglomerates at the tight junction was measured as half-width of peaks obtained by plotting the fluorescence intensity profiles across the cell boundary.

In vivo experimental design

The study was conducted on female Wistar rats. The animals were introduced into the experiment when they were 6–8 weeks old, which is the period of their full sexual maturity and mineralization of bone tissue. During the experiment, the animals were fed and watered *ad libitum* and were exposed to light and darkness regimen in duration of 12 hours for each period. Animals were divided into two groups, so that one group of 8 animals was the control (K), and a second one was experimental (E). The latter group consisted of 40 animals, all of which were treated with glucocorticoids in order to induce osteoporosis. The animals were given two types of glucocorticoids: methylprednisolone Na-succinate (Lemod Solu, Hemofarm Vršac, Serbia) at 2 mg per kg of body weight, and dexamethasone-Na-phosphate (Dexason, ICN Galenika, Belgrade, Serbia) at 0.2 mg per kg of body weight. These osteoporosis-inducing agents were administered intramuscularly and alternating for 12 weeks, so that every day the animals were given a different glucocorticoid. A model of osteoporosis of rat mandible wherein osteoporosis was formed after such treatment was presented in our previous articles [25, 26]. Animals from the control group received daily intramuscular saline solution during this specified 12-week period.

At the end of 12 weeks, defects were created on the left side of the alveolar bone of mandible, in the region between the midline and the mental foramen, in all the animals. The defects were made using sterile steel borer with 1.6 mm in diameter and 1.8 mm in length, which was smaller than the critical size because it was necessary to avoid the risk of fracture that osteoporotic bone is susceptible to. The animals were prepared for this intervention with an injection of diazepam (Bensendin, ICN Galenika, Belgrade, Serbia) and the subsequent induction of anesthesia using ketamine hydrochloride USP (Ketalar, Rotexmedica Gmbh, Trittau, Germany).

The animals from group E were divided into 5 subgroups (each consisting of 8 animals) for implantation of the following nanostructured powders: HAp, HAp/Co1, and HAp/Co2. HAp/Co2 powder was also applied after being admixed to autologous blood and autologous blood plasma. All three samples were mixed prior to implantation with saline (0.9% NaCl solution). The weight ratio of autologous blood or blood plasma and the admixed HAp/Co2 powder was 2:1. The plasma was prepared following a procedure described in the literature [25]. The mandibular defects in rats from group K were not filled, but were left to heal spontaneously, so as to provide a reference to compare the osteoporotic bone regeneration aided by the implanted nanoparticles to. The animals in both groups (E and K) were

sacrificed 6 and 24 weeks after the implantation since previous studies have shown that best results can be expected during this period [26, 27]. The procedures involving experimental animals were done in accordance with the *Guidelines for Work with Experimental Animals* adopted by the Ethics Committee of the Faculty of Medicine, University of Niš, Serbia. After 6 and 24 weeks of implantation, samples of the alveolar bone were decalcified, dehydrated in a series of alcohol and embedded in paraffin blocks (n = 5 for each animal). Of these blocks were made 10-μm-thin slides, which were then stained by H&E and Masson's Trichrome Kit for histopathological analysis, with the minimum of three slides per staining [25, 28]. The microscopic analysis of the defect area and its immediate surroundings in the healthy and osteoporotic bone was performed. After the specified time (6 and 24 weeks) blood samples were taken for a biochemical analysis and alkaline phosphatase (ALP) activity was determined on an Olympus AU 680 analyzer according to a standard method presented in the literature [29]. After the same treatment times a change in the local bone mineral density (BMD) of jaw was measured using the dental scanner for computerized tomography [30, 31]. The density was determined at the site of the defect with a depth of 1.8 mm and on the surface area of 3 mm^2, which included both the area of the defect and its bone boundary. The control was a healthy bone of untreated rats determined under the same conditions. BMD measurements in Hounsfield units were carried out using the scanning protocol described by Homolka et al. [32], modified to fit the size of the object. The results were statistically analyzed by MANOVA test.

Results and discussion

Fig. 1a shows XRD patterns of the materials used in this study (HAp, HAp/Co1, and HAp/Co2), demonstrating that all of them consisted of pure, monophasic apatite. Ritvield crystallographic analysis and Raman spectroscopy confirmed replacement of Ca^{2+} ions with Co^{2+} ions in the crystal lattice of HAp during the hydrothermal synthesis [23]. The partial Ca^{2+}-to-Co^{2+} substitution entailed a reduction in the unit cell volume, from 529 A^3 for HAp to 524 A^3 for HAp/Co2, as well as a reduction in the average crystallite size, from 40 nm for HAp to 26 nm for HAp/Co1 to 14 nm for HAp/Co2, as indicated by the broadening of the diffraction lines in direct proportion with the content of Co^{2+} ions in HAp/Co [16]. The particle size distribution profiles for different samples are shown in Fig. 1b. The median diameters of primary particles were calculated to be 94, 63 and 71 nm for HAp, HAp/Co1 and HAp/Co2, respectively. The introduction of Co^{2+} ions to HAp lattice not only decreases the crystallite size, lowers crystallinity and affects the particle morphology, but it also promotes agglomeration in direct proportion with an increase in the content of Co^{2+} [16, 23]. Consequently, HAp/Co1 has the smallest mean particles size. SEM images of HAp and HAp/Co1 samples are shown in Fig. 1c–d, demonstrating a considerable extent of agglomeration in both samples as well as a difference in the particle size and morphology brought about by incorporation of Co^{2+} ions into the crystal structure of HAp.

Fig. 2 demonstrates no significant damage done by HAp particles with the largest content of Co (HAp/Co2) to the epithelial monolayers of Caco-2 cells under the given experimental conditions, as evidenced by the preserved cobblestone pattern of ZO-1 molecules. ZO-1 is a perijunctional protein that acts as a link between actin cytoskeletal microfilaments and the transmembrane proteins of the tight junction [33]. Any toxic effects exhibited by the particles would appear as either discontinued or extensively ruffled ZO-1 pattern. Although ruffling of the ZO-1 pattern was observed following incubation with Co-substituted HAp (Fig. 2b), the integrity of the tight junction was preserved. Certain drugs were also shown to negatively affect epithelial monolayers by inducing focal aggregation of the tight junction proteins, including ZO-1, and their colocalization with the disrupted cytoskeletal filaments along the cell boundaries [34]. This effect was, however, not observed upon the application

of Co-substituted HAp. No significant change with respect to the negative control was observed either in the thickness of ZO-1 conglomerates at the tight junction.

Incubation of HAp/Co particles however produced a somewhat unviable response by the osteoblastic cells. As shown in Fig. 3b–c, f-actin microfilaments in some cells appeared partially disrupted, lacking the striated appearance of the negative control (Fig. 3a). Cytoskeleton of other cells appeared relatively healthy, although their density was markedly diminished (Fig. 3d). A portion of cells, especially those in direct contact with the particles, clearly displayed apoptotic morphologies (Fig. 3e). Despite that, the osteoblastic cells were observed to be well spread (Fig. 3f), suggesting the dual effect of the particle surface: osteoconductivity on one side and moderate toxicity on the other. Inhibited proliferation of cells was detected in the presence of all HAp/Co particles, as apparent from the lower cell density in comparison with the control sample. Mineralization centers were, however, still observed within the cells, indicating their continued mineralization activity. Furthermore, the results of the MTT assay shown in Fig. 4 demonstrate a decrease in the mitochondrial activity of the cells, indicative of the cell viability, in direct proportion with the Co content in HAp/Co particles, from 5 wt% (HAp/Co1) to 9 wt% to 12 wt% (HAp/Co2). Moderate cytotoxicity of cobalt ions and nanoparticles has been demonstrated previously in various *in vitro* studies [35], and Co^{2+} levels of around 400 μM were shown to correspond to IC50 values for apoptosis of C6 glioma cells [36]. Dose-dependent cytotoxicity, in agreement with our findings, was also previously observed during dosage of Vero cells with cobalt chloride [37]. A study aimed to evaluate the released amount of a range of divalent cationic substitutes from HAp in cell culture media has come to conclusion that the second largest released amount is that of Co^{2+}, only surpassed by Cu^{2+} [38]. In the latter study, the amount of macrophages identified positively for apoptosis reached 100 % when incubated with Co-substituted HAp, while at the same time osteoblasts adhered to Co-substituted HAp better than to any other divalent-cation-substituted HAp, a result consistent with our findings.

Whereas toxicity of cobalt ions has been regularly demonstrated on cell cultures, less evident has been toxicity of cobalt to whole organisms [39] exposed to small to moderate amounts thereof, although there are cases documented in the literature [40, 41, 42]. In any case, while Co^{2+} ions released from HAp/Co particles in cell culture conditions are nowhere as rapidly cleared as in the body, higher levels of toxicity are naturally expected in the former case, and our *in vivo* findings, demonstrating favorable regeneration of osteoporotic bone treated with the paramagnetic HAp/Co, are supportive of this observation.

Fig. 5 shows the histopathology of alveolar bone 6 weeks after the implantation. Histopathological slides of the sections of mandible from the control group (Fig. 5a) reveal homogeneous areas without holes, representing compact bone, and an area with numerous interconnected cavities, representing cancellous bone. The compact part of the alveolar bone shows usual collagenesis and osteogenesis for the given healing interval. Overall, the control samples exhibited normal bone texture, in both its compact and cancellous parts. In Fig. 5b, one could see the ongoing destruction of the implanted nanomaterial and the formation of young bone in the proximity of the defect wherein the biomaterial was implanted. In Fig. 5c, one can spot an area of mandibular bone covered with a layer of periosteum and a layer of connective tissue. Filling of the defect with the newly formed bone typified by intense angiogenesis is seen along the edges. Replacement of the implanted nanomaterial with this young bone, discernable by distinct cement lines and islets of fibrous tissue, can also be seen from Fig. 5d. Large blood vessels (diameter>30 μm) were somewhat present in all the specimens, whereas an abundance of capillaries was observed, especially when HAp/Co2 was applied. The blood vessels were seen 24 weeks after the implantation and their average number in 8×10^6 μm^2 surface section area was 1.78±1.39, 2.33±2.00, 2.67±1.00 and 3.33±1.22 for K, HAp, HAp/Co1, and HAp/Co2 samples, respectively. These results

indicate an intense process of angiogenesis and filling of the defects with young bone 6 weeks after the implantation of HAp/Co2 material. Angiogenesis plays an important role in the formation of bone tissue during the reparation of bone fractures and was more intense for HAp/Co2 compared to other analyzed materials (HAp, HAp/Co1).

Fig. 6 shows the histopathology of alveolar bone 24 weeks after the implantation. In the control group (Fig. 6a), an even more intense formation of the new bone is seen as well as rapid incorporation of Ca^{2+} into the existing bone matrix, indicating the ongoing mineralization. Bone regenerated in the presence of Co-free HAp implants (Fig. 6b) demonstrates resorption and replacement of the implanted material paralleled by osteogenesis and bone regeneration. Continuation of defect ossification is observed for HAp/Co samples too and for HAp/Co1 the bone defect appears to be completely filled with the new bone (Fig. 6c). The presence of collagen, Haversian canals, cement lines as well as the beginning of ossification and calcification can be observed. Angiogenesis, the thick cement lines, a number of Haversian canals, a vast number of osteogenesis cells in the process of calcification and obturations of the artificial defect were also seen in the mandibular specimens regenerated in the presence of HAP/Co2 (Fig. 6d). These observations suggest that vascularization is essential during osseointegration because it directly affects the processes of differentiation and ossification of bone tissue. These processes affect remodeling, adaptation and consolidation of the newly formed bone, which can last for several months [41]. Osteogenesis observed after 24 weeks of implantation of HAp/Co2 material (Fig. 6d) is very similar to that present in healthy bone tissue [43].

The content of ALP and alveolar bone density measured 6 and 24 weeks after the reconstruction of osteoporotic bone has been initiated are given in Fig. 7. The highest density of alveolar bone, although not statistically significant in comparison with the control (K), was detected for bone regenerated by means of HAp/Co2, the material that was further on mixed with blood and blood plasma to investigate its potential for improving regenerative processes to a greater extent. The blood levels of ALP, a mineralization marker, were markedly higher for all HAp materials, with and without Co, with respect to the control, as in agreement with the greater degree of ossification observed in the given samples when compared to the control.

Fig. 8 shows the histopathology of alveolar bone 6 and 24 weeks after the reconstruction with HAp/Co2 mixed with either blood or blood plasma. The sample regenerated by means of HAP/Co2/blood (Fig. 8a) shows minimal residues of the implanted material 6 weeks after the reconstruction as well as the ongoing replacement of the implanted material with the connective tissue and the onset of ossification. After 24 weeks, the activity of osteogenic cells, the presence of young bone and a portion of mature calcified bone in its vicinity could be additionally seen (Fig. 8c). A decent blood supply and the presence of Haversian systems with cement lines, numerous collagen fibers, along with a similarly accelerated replacement of the implanted material by the newly formed bone can also be seen in the sample regenerated by means of HAP/Co2/blood after 6 weeks (Fig. 8b). After 24 weeks, observable are the areas of ossification utilizing giant cells, while newly formed bone is present as well as a number of cement lines, Haversian canals with mature bone around them and numerous foci of calcification (Fig. 8d).

ALP, a specific biomarker of osteogenesis, as well as bone densities show a significant increase when HAp/Co2 materials is implanted together with saline solutions, blood and blood plasma (Fig. 9). The highest values of both ALP and bone density were detected when HAp/Co2 was mixed with blood plasma before its application, as in consistency with the previously presented histopathological results. ALP values increased between 6 and 24 weeks after the reconstruction, which may be caused by an imbalance in bone metabolism

and increased bone resorption, a process similar to premenopausal and early menopause changes [44, 45]. These changes are also due to sufficient time existent for the growth factors, present in autologous blood and plasma, to associate with the osteogenic activity of nanoparticles [13]. This, in turn, leads to significant changes in bone regeneration via an increased excretion of ALP from the osteoblasts, more active when the bone matrix is deposited in the phase of bone reconstruction.

The obtained results demonstrate the ability of Co-substituted HAp to accelerate (a) osteogenesis and regeneration of osteoporotic bone, and (b) replacement of the implanted material with a newly formed bone. Mild inflammation is known to ensue every facile resorption of a biomaterial used in tissue reparation and a larger inflammatory capacity of HAp/Co particles compared to HAp ones could have been an osteogenesis-promoting factor in this case. Moderate cytotoxicity of the material could also facilitate the transport of Ca^{2+} ions in the intracellular fluid, further stimulating the osteogenic activity of osteoblasts. Cobalt-substituted HAp could also induce cytokine production, which might lead to enhanced exchange across the cell membrane. In the endoplasmatic reticulum, this could lead to changes in acid/base balance, which might enhance the activity of aminopeptidases and lead to an increased proliferation and migration of endothelial cells, a factor of vital importance for the process of osteogenesis.

HAp/Co2 mixed with blood or autologous plasma, rich in growth factors, also induces generation of a large number of osteoblasts, leading to faster regeneration of osteoporosis-weakened bone. This process entails a more rapid incorporation of mineral ions into HAp crystal lattice of the newly formed bone. As the result, the process of intense mineralization can be clearly observed 24 weeks after the reconstruction. Osteogenesis and regeneration of the reconstructed defect 24 weeks after the implantation of HAp/Co2 material mixed with autologous plasma (Fig. 8b) is very pronounced and the newly formed bone appears to be identical to healthy bone. It is likely that the mononuclear cells are stimulated by the growth factors from autologous blood and plasma as well as by the presumed increased production of cytokines induced by Co^{2+} ions, so that they transform into macrophages turned active and of greater capacity for phagocytosis due to an increased concentration of lysosomal enzymes. The given stimuli produce migration and proliferation of fibroblasts, stimulation of collagen synthesis and activation and synthesis of metalloproteinases, enzymes that participate in restructuring the extracellular matrix. These phenomena can be envisaged to result in bone remodeling, adhesion, cell migration and multiplication of bone-forming cells, including eventually full mineralization and mature bone formation at the site of the defect. The synergetic effect of growth factors and thrombocytes from autologous plasma with HAp/Co2 has thus led to an increased proliferation and migration of active cells that rapidly obturate the artificial defect and improve the osteoporotic bone regeneration, as noted previously [46].

Conclusion

The possibility of reconstruction of osteoporotic bone defects of the mandible using hydroxyapatite and cobalt-substituted hydroxyapatite nanoparticles was investigated. Biocompatibility tests carried out on cell cultures have shown intact monolayers of epithelial cells in contact with cobalt-substituted hydroxyapatite and no negative effects on the cell viability. In contrast, prolonged incubation of the given material with osteoblastic cells *in vitro* resulted in partial morphological and cytoskeletal deformation of the cells as well as a decrease in their viability in direct proportion with the content of cobalt ions incorporated in the crystal lattice of hydroxyapatite. In contrast, an increase in the amount of calcium ions substituted by cobalt, up to 12 wt%, corresponded to an increase in the rate of osteogenesis and formation of the newly formed and mature calcified bone. After 24 weeks of

reconstruction using nanosized cobalt-substituted hydroxyapatite with 12 wt% of cobalt ions, an intense angiogenesis, vascularization, migration and multiplication of bone-forming cells as well as maximal values of alkaline phosphatase and bone density have been achieved. The combined effect of growth factors from autologous blood plasma and cobalt-substituted hydroxyapatite had a crucial effect on the observed increase in cell proliferation and migration of active cells that rapidly obturate the artificial defects, improve osteoporotic bone regeneration and increase the bone density of the mandible.

Acknowledgments

The research presented in this paper was supported by the Ministry of Education and Science of the Republic of Serbia under the Project No. III45004 and by the NIH/NIDCR grant K99-DE021416. Confocal microscopy data for this study were acquired at the Nikon Imaging Center at University of California, San Francisco. FE-SEM images were obtained by courtesy of Dr. Srečo Škapin from Jožef Stefan Institute. Authors would also like to thank MSc. Ljilijana Veselinović for XRD measurements.

References

1. Raisz LG. Pathogenesis of osteoporosis: concepts, conflicts, and prospects. J Clin Invest. 2005; 115:3318–3325. [PubMed: 16322775]
2. Pollähne W, Pfeifer M, Lazarescu A, Minne HW. Osteoporose: Bildgebende Diagnostik. Medizin im Bild. 1996; 3:37–44.
3. Marco F, Milena F, Gianluca G, Vittoria O. Peri-implant osteogenesis in health and osteoporosis. Micron. 2005; 36(7–8):630–644. [PubMed: 16182543]
4. Gupta AK, Gupta M. Synthesis and surface engineering of iron oxide nanoparticles for biomedical applications. Biomaterials. 2005; 26(18):3995–4021. [PubMed: 15626447]
5. Ito A, Honda H, Kobayasji T. Cancer immunotherapy based on intracellular hyperthermia using magnetite nanoparticles: a novel concept of “heat-controlled necrosis” with heat shock protein expression. Cancer Immunol Immunother. 2006; 55(3):320–328. [PubMed: 16133113]
6. Hench LL. Bioceramics. J Am Ceram Soc. 1998; 81(7):1705–1728.
7. Le Geros RZ, Craig RG. Strategies to affect bone remodeling: osteointegration. J Bone Miner Res. 1993; 8(2):S583–596. [PubMed: 8122530]
8. Ajdukovic Z, Ignjatovic N, Petrovic D, Uskokovic D. Substitution of osteoporotic alveolar bone by biphasic calcium phosphate/poly –DL-lactide–co-glycolide biomaterials. J Biomat Appl. 2007; 21(3):317–328.
9. Ignjatovic N, Uskokovic D. Biodegradable composites based on nano-crystalline calcium phosphate and bioresorbable polymers. Adv Appl Ceram. 2008; 107:142–147.
10. Abdel-Fattah, Wafaa I.; Osiris, WG.; Mohamed, Shamael S.; Khalil, MR. Reconstruction of resected mandibles using a hydroxyapatite veterinary bone graft. Biomaterials. 1994; 15(8):609–614. [PubMed: 7948580]
11. Tami, Andrea E.; Leitner, Melanie M.; Baucke, Michelle G.; Mueller, Thomas L.; Harry van Lenthe, G.; Müller, Ralph; Ito, Keita. Hydroxyapatite particles maintain peri-implant bone mantle during osseointegration in osteoporotic bone. Bone. 2009; 45(6):1117–1124. [PubMed: 19679208]
12. Verron, Elise; Gauthier, Olivier; Janvier, Pascal; Pilet, Paul; Lesoeur, Julie; Bujoli, Bruno; Guicheux, Jerome; Bouler, Jean-Michel. In vivo bone augmentation in an osteoporotic environment using bisphosphonate-loaded calcium deficient apatite. Biomaterials. 2010; 31(30): 7776–7784. [PubMed: 20643480]
13. Ignjatovic N, Ajdukovic Z, Savic V, Uskokovic D. Size effect of calcium phosphate coated with poly-(DL-lactide-co-glycolide) on healing processes in bone reconstruction. Journal of Biomedical Materials Research Part B: Applied Biomaterials. 2010; 94B:108–117.
14. Balasundaram, Ganesan; Sato, Michiko; Webster, Thomas J. Using hydroxyapatite nanoparticles and decreased crystallinity to promote osteoblast adhesion similar to functionalizing with RGD. Biomaterials. 2006; 27(14):2798–2805. [PubMed: 16430957]

15. Uskoković V, Uskoković DP. Nanosized hydroxyapatite and other calcium phosphates: Chemistry of formation and application as drug and gene delivery agents. Journal of Biomedical Materials Research B: Applied Biomaterials. Jan.2011 96B(1)
16. Veselinovic, Lj; Karanovic, Lj; Stojanovic, Z.; Bracko, I.; Markovic, S.; Ignjatovic, N.; Uskokovic, D. Crystal structure of cobalt-substituted calcium hydroxyapatite nanopowders prepared by hydrothermal processing. Journal of Applied Crystallography. 2010; 43:320–327.
17. Zhang JM, Lin CJ, Feng ZD, Tian ZW. Hydroxyapatite/metal composite coatings prepared by multistep electrodepozition method. Journal of Materials Science Letters. 1998; 17:1077–1079.
18. El Ouassouli A, Ezzemouri S, Ezzamarty A, Lakhdar M, Leglise J. Catalyseurs sulfures à base de cobalt et d'hydroxyapatite. J Chim Phys. 1999; 96(7):1212–1225.
19. Landi, Elena; Tampieri, Anna; Celotti, Giancarlo; Sprio, Simone; Sandri, Monica. Giandomenico Logroscin, Sr-substituted hydroxyapatites for osteoporotic bone replacement. Acta Biomaterialia. 2007; 3(6):961–969. [PubMed: 17618844]
20. Meng J, Zhang Y, Qi X, Kong H, Wang C, Xu Z, Xie S, Gu N, Xu H. Paramagnetic nanofibrous composite films enhance the osteogenic responses of pre-osteoblast cells. Nanoscale. 2010; 2:2565–2569. [PubMed: 20949222]
21. Li Y, Nam CT, Ooi CP. Iron(III) and manganese (II) substituted hydroxyapatite nanoparticles: characterization and cytotoxicity analysis. J Phys: Conf Ser. 2009; 187:012024.
22. Patel, Bhairav; Favaro, Gregory; Inam, Fawad; Reece, Michael J.; Angadji, Arash; Bonfield, William; Huang, Jie; Edirisinghe, Mohan. Cobalt-based orthopaedic alloys: Relationship between forming route, microstructure and tribological performance. Materials Science and Engineering C. 201210.1016/j.msec.2012.03.012;
23. Stojanovic Z, Veselinovic Lj, Markovic S, Ignjatovic N, Uskokovic Dragan. Hydrothermal Synthesis of Nanosize Pure and Cobalt-exchanged Hydroxyapatite. Materials and Manufacturing Processes. 2009; 24:1096–1103.
24. Uskoković, Vuk; Lee, Phin Peng; Walsh, Laura; Fischer, Kathleen E.; Desai, Tejal A. Silicon Nanowire Coated Microparticles as Epithelial Drug Delivery Devices. The Effect of PEGylation on Particle-Epithelium Interactions. Biomaterials. 2012; 33(5):1663–1672. [PubMed: 22116000]
25. Ajdukovic Z, Najman S, Djordjevic Lj, Savic V, Mihailovic D, Petrovic D, Ignjatovic N, Uskokovic D. Repair of bone tissue affected by osteoporosis with hydroxyapatite-poly-L-(HAp/PLLA) with and without blood plasma. J Biomat Appl. 2005; 20(2):179–190.
26. Ignjatovic N, Ajdukovic Z, Uskokovic D. New biocomposite calciumphosphate/poly-DL-lactide-co-glycolide/biostimulatite agens filler for reconstruction of bone tissue changed by osteoporosis. Journal of Materials Sciences: Materials in Medicine. 2005; 16:621–626.
27. Ignjatovic N, Ninkov P, Ajdukovic Z, Vasiljevic-Radovic D, Uskokovic D. Biphasic calcium phosphate coated with poly-D,L-lactide-co-glycolide biomaterial as a bone substitute. J Europ Ceram Soc. 2007; 27(2–3):1589–159.
28. Miao D, Scutt A. Histochemical localization of alkaline phosphatase activity in decalcified bone and cartilage. J Histochemistry & Cytochemistry. 2002; 50(3):333–340.
29. Britti D, Massimini G, Peli A, Luciani A, Boari A. Evaluation of serum enzyme activities as predictors of passive transfer status in lambs. J Am Vet Med Assoc. 2005; 226(6):951–955. [PubMed: 15786999]
30. Macleod I, Heath N. Cone-beam computed tomography (CBCT) in dental practice. Dent Update. 2008; 35:590–598. [PubMed: 19065875]
31. Suomalainen A, Kiljunen T, Käser Y, Peltola J, Kortesniemi M. Dosimetry and image quality of four dental cone beam computed tomography scanners compared with multislice computed tomography scanners. Dentomaxillofac Radiol. 2009; 38(6):367–378. [PubMed: 19700530]
32. Homolka P, Beer A, Birkfellner W, Nowotny R, Gahleitner A, Tschabitscher M, Bergmann H. Bone Mineral Density Mesaurement with Dental Quantitative CT Prior tu Dental Implant Placement in Cadaver Mandibles: Pilot Study. Radipoly. 2002; 224(1):247–252.
33. Fanning AS, Jameson BJ, Jesaitis LA, Anderson JM. The Tight Junction Protein ZO-1 Establishes a Link between the Transmembrane Protein Occludin and the Actin Cytoskeleton. Journal of Biological Chemistry. 1998; 273:29745–29753. [PubMed: 9792688]

34. Wittchen ES, Haskins J, Stevenson BR. Protein interactions at the tight junction. Actin has multiple binding partners, and ZO-1 forms independent complexes with ZO-2 and ZO-3. Journal of Biological Chemistry. 1999; 274:35179–35185. [PubMed: 10575001]
35. Horev-Azaria L, Kirkpatrick CJ, Korenstein R, Marche PN, Maimon O, Ponti J, Romano R, Rossi F, Golla-Schindler U, Sommer D, Uboldi C, Unger RE, Villiers C. Predictive toxicology of cobalt nanoparticles and ions: comparative in vitro study of different cellular models using methods of knowledge discovery from data. Toxicological Sciences. 2011; 122(2):489–501. [PubMed: 21602188]
36. Yang SJ, Pyen J, Lee I, Lee H, Kim Y, Kim T. Cobalt chloride-induced apoptosis and extracellular signal-regulated protein kinase 1/2 activation in rat C6 glioma cells. Journal of Biochemistry and Molecular Biology. Jul 3; 2004 1 37(4):480–6. [PubMed: 15469737]
37. Gürbay A. Protective Effect of Zinc Chloride Against Cobalt Chloride-Induced Cytotoxicity on Vero Cells: Preliminary Results. Biological Trace Element Research. 2012 Jan 27. [Epub ahead of print];
38. de Lima IR, Alves GG, Soriano CA, Campaneli AP, Gasparoto TH, Ramos ES Jr, de Sena LÁ, Rossi AM, Granjeiro JM. Understanding the impact of divalent cation substitution on hydroxyapatite: an in vitro multiparametric study on biocompatibility. J Biomed Mater Res A. 2011 Sep 1; 98(3):351–8. Epub 2011 May 27. 10.1002/jbm.a.33126 [PubMed: 21626666]
39. Lantin AC, Mallants A, Vermeulen J, Speybroeck N, Hoet P, Lison D. Absence of adverse effect on thyroid function and red blood cells in a population of workers exposed to cobalt compounds. Toxicology Letters. Feb 25; 2011 201(1):42–6. Epub 2010 Dec 21. [PubMed: 21182909]
40. Pelclova D, Sklensky M, Janicek P, Lach K. Severe cobalt intoxication following hip replacement revision: Clinical features and outcome. Clinical toxicology (Philadelphia, Pa). Apr; 2012 50(4): 262–5.
41. Hallab NJ, Chan FW, Harper ML. Quantifying subtle but persistent peri-spine inflammation in vivo to submicron cobalt-chromium alloy particles. European Spine Journal. 2012 Mar 10. [Epub ahead of print];
42. Gill HS, Grammatopoulos G, Adshead S, Tsialogiannis E, Tsiridis E. Molecular and immune toxicity of CoCr nanoparticles in MoM hip arthroplasty. Trends in Molecular Medicine. Mar; 2012 18(3):145–55. [PubMed: 22245020]
43. Ratner, DB.; Hoffman, AS.; Schoen, FJ.; Lemons, JE. An Introduction to Materials in Medicine. 2. Elsevier Academic Press; San Diego, California, USA: 2004. Biomaterials science; p. 23-40.
44. Seibel JM. Biochemical markers of Bone Turnover Part II: Clinical Applications in the Management of Osteoporosis. Clin Biochem Rev. 2006; 27(3):123–138. [PubMed: 17268581]
45. Meunier PJ, Jenvrin C, Munoz F, de la Gueronniere V, Garnero P, Menz M. Consumption of a high calcium mineral water lowers biochemical indices of bone remodeling in postmenopausal women with low calcium intake. Osteoporos Int. 2005; 16(10):1203–1209. [PubMed: 15744450]
46. Hen-Yu L, Alexander WTH, Ching-Yu T, Kuei-Ru C, Rong Z, Ming-Fu W, Wen-Chang C, Shiaw-Min H, Ching-Hua S, Win-Ping D. The balance between adipogenesis and osteogenesis in bone regeneration by platelet-rich plasma for age-related osteoporosis. Biomaterials. 2011; 32:6773–6780. [PubMed: 21700330]

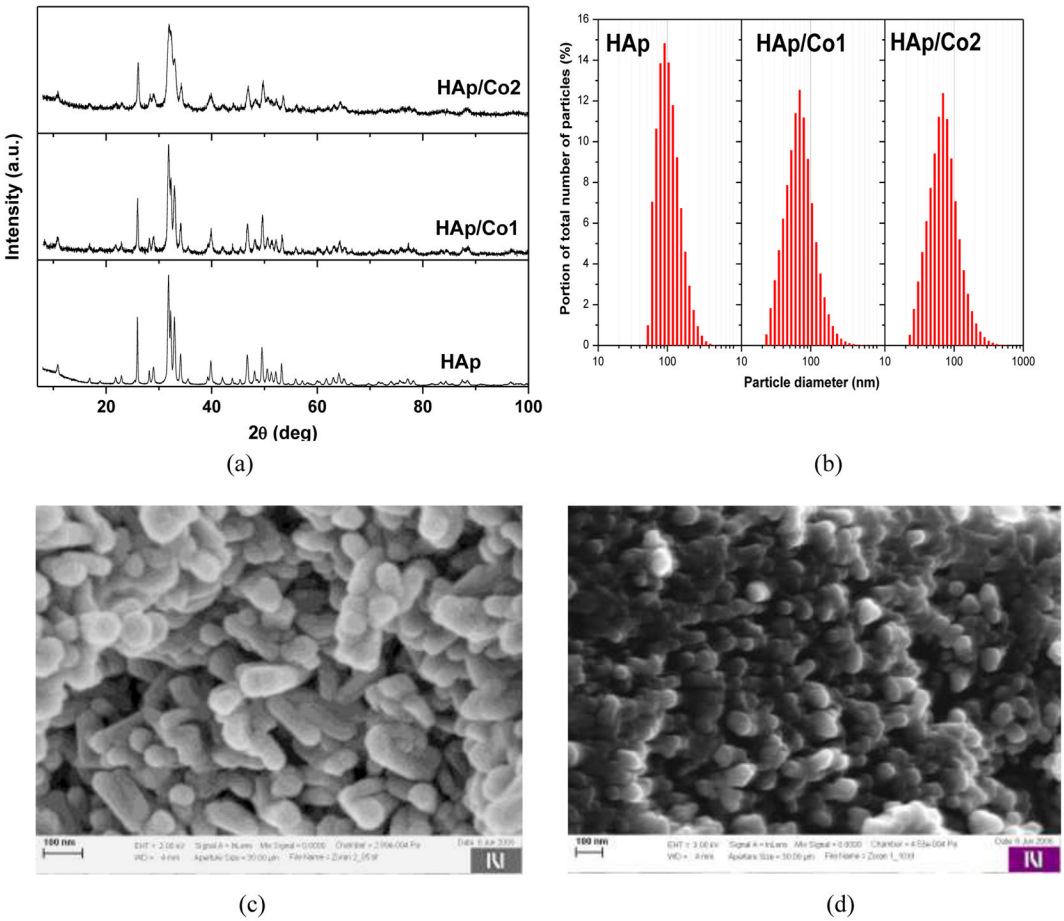

Fig. 1.

a) XRD patterns of synthesized materials; b) size distribution of particles obtained by LD; c) and d) SEM images of nanopowder samples HAp and HAp/Co1, respectively.

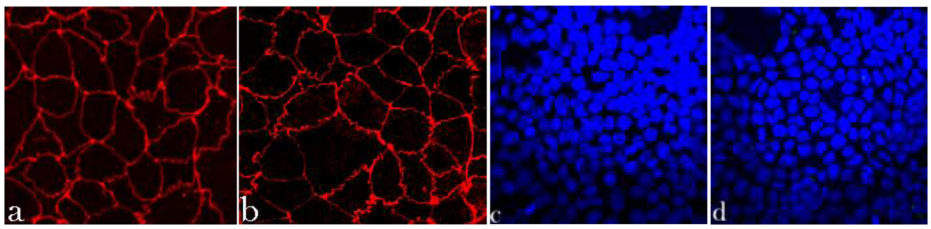

Fig. 2.

Immunofluorescent staining of ZO-1 molecules (a–b) and cell nucleus (c–d) in Caco-2 cell monolayers treated with either no particles (control, a, c) or 2 mg/cm^2 of HAp/Co2 particles (b, d), imaged under identical excitations. The sizes of images (a, b) and (c, d) is 200 × 200 μm and 475 × 475 μm, respectively.

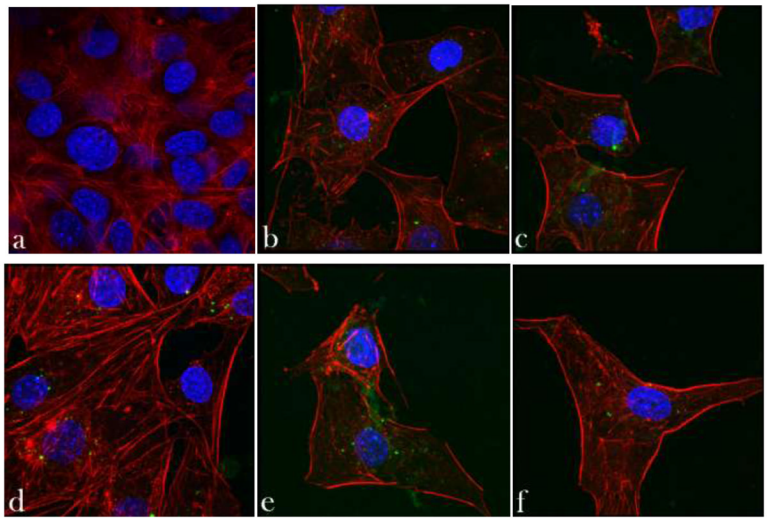

Fig. 3.

Confocal optical micrographs of fluorescently stained osteoblastic cell nucleus (blue) and cytoskeletal f-actin (red), and HAp/Co particles and/or intracellular mineral particles (green) following 7 days of incubation with either no particles (control, a) or 2 mg/cm^2 of HAp/Co particles (b–f). The size of each image is 750 × 750 μm.

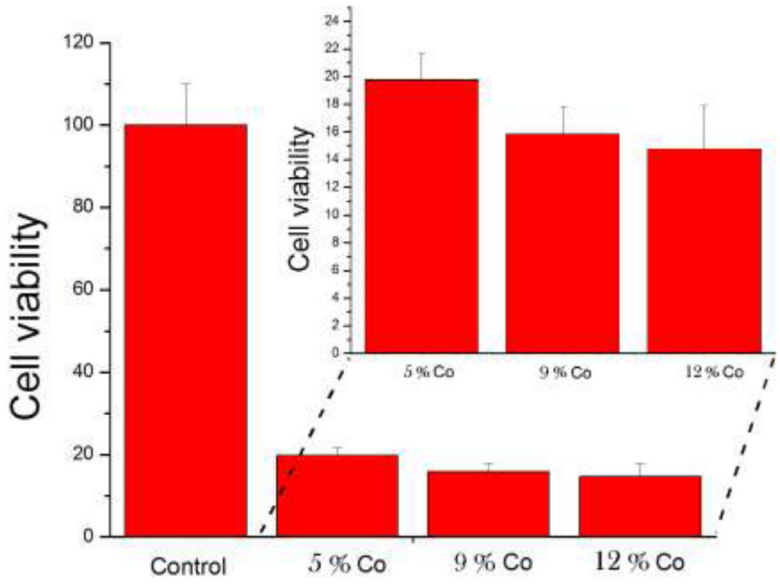

Fig. 4.

Mitochondrial activity indicative of cell viability, normalized to the negative control (C−) and determined by the MTT assay for HAp/Co particles containing different weight percentage of Co^{2+} ions: 5 wt% (HAp/Co1), 9 wt% and 12 wt% (HAp/Co2).

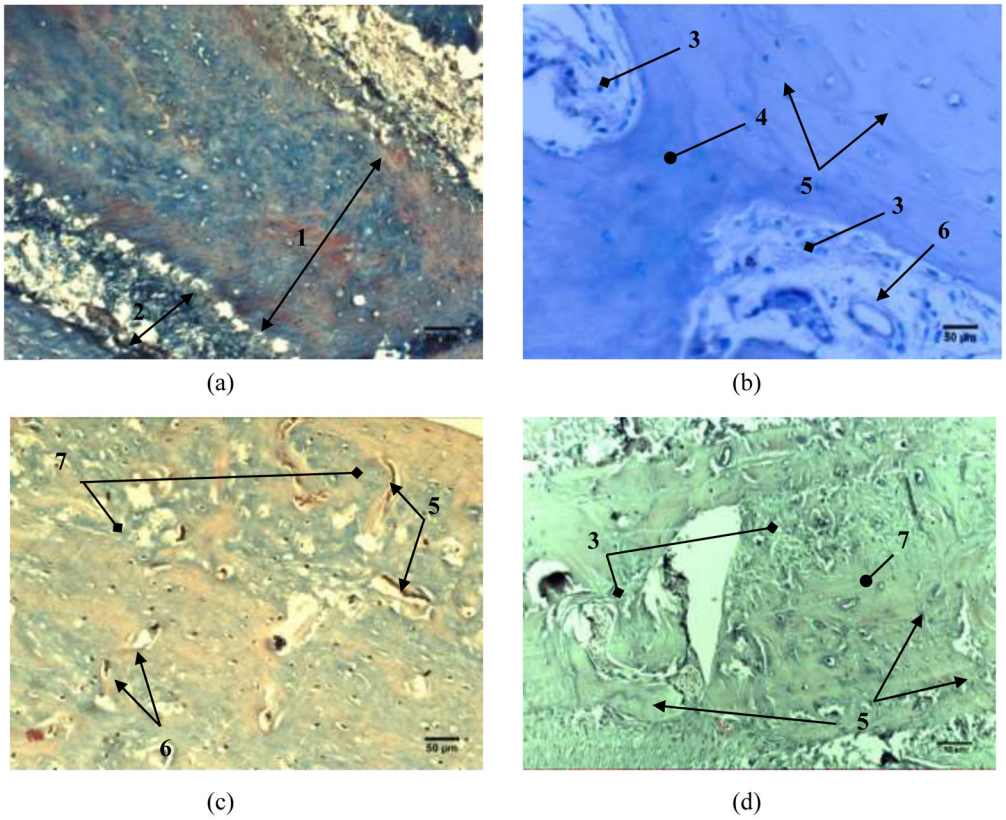

Fig. 5.

Histopathology of alveolar bone 6 weeks after the implantation: a) control group, b) HAp; c) HAp/Co1 and d) HAp/Co2. [labels: 1 - compact bone, 2 - cancellous bone, 3 - replacement of the material with new bone tissue, 4 - a young bone, 5 - cement lines, 6 - blood vessel, 7 - the newly formed bone]

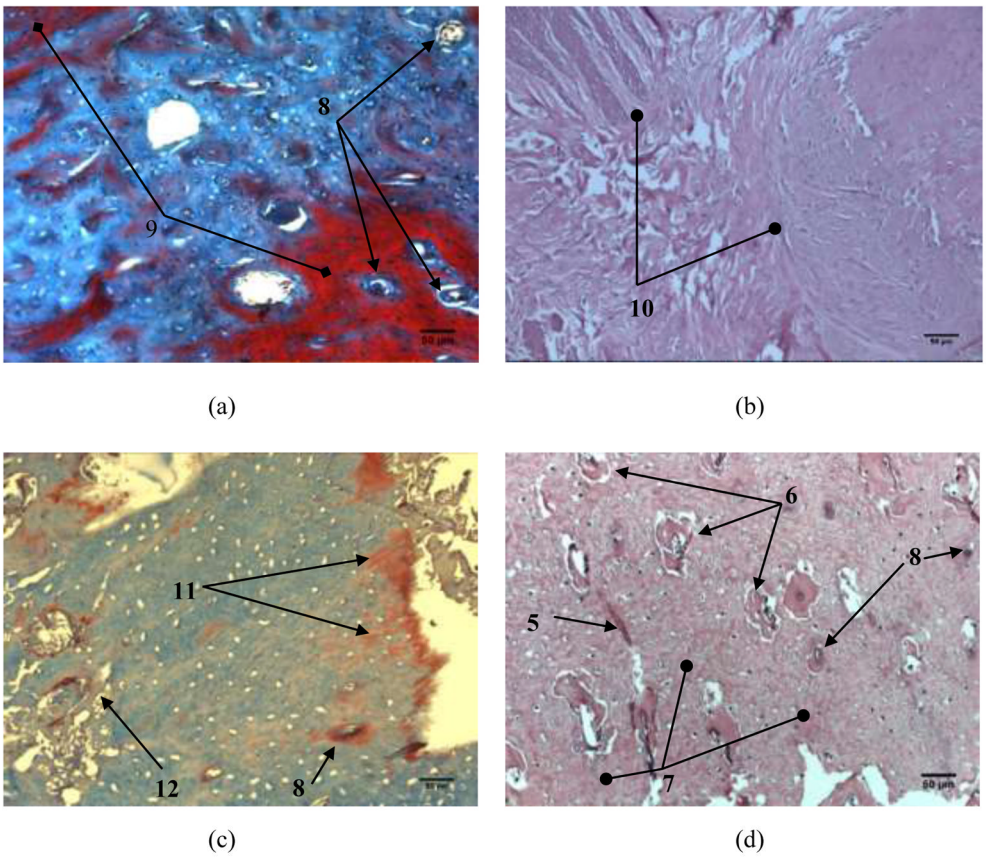

Fig. 6.

Histopathology of alveolar bone 24 weeks: a) control group, b) HAp; c) HAp/Co1; d) HAp/Co2. [labels: 5 - cement lines, 6 - blood vessel, 7 - the newly formed bone, 8 - Haversian canals, 9 - bone mineralization, 10 - osteogenesis, 11 - the beginning of ossification and calcification, 12 - collagen fibers, 13 - mature calcified bone]

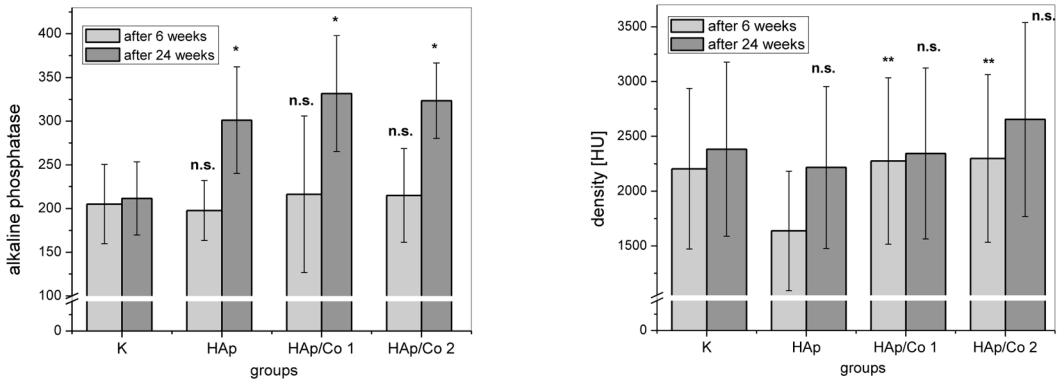

Fig. 7.

(a) ALP content (U/L) and (b) densities of alveolar bone expressed in Haunsfiled units (HU), 6 and 24 weeks after the implantation, for different experimental groups (HAp, HAp/Co1, HAp/Co2) and the control (K). K indicates healthy bone in (b). Data are shown as means with error bars representing standard deviation (* => $p < 0.01$ with respect to the control group; ** => $p < 0.05$ with respect to HAp group, n.s. => non-significant with respect to the control group).

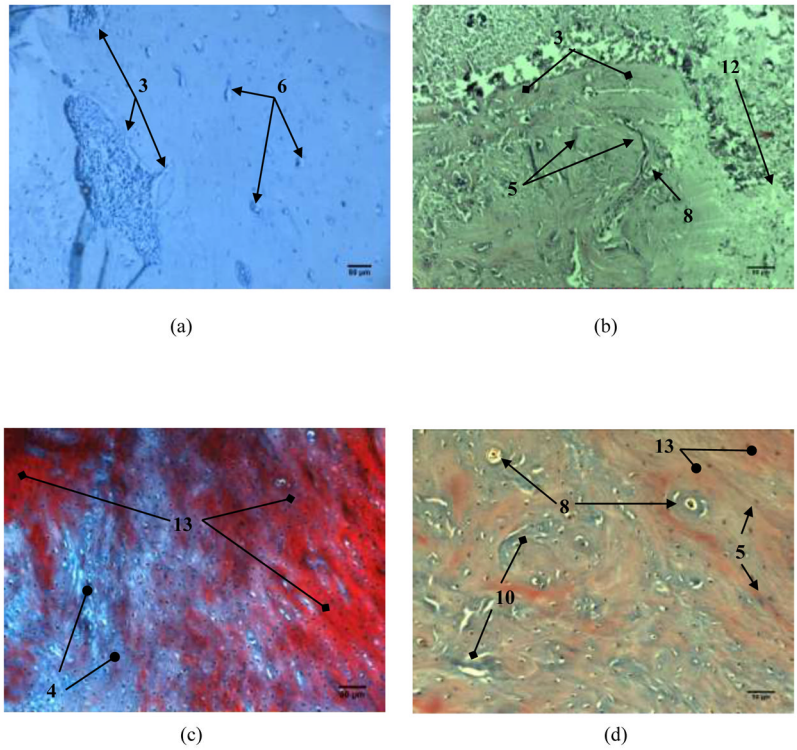

Fig. 8.

The histopathology of alveolar bone reconstructed with HApCo2 after 6 (a, b) and 24 weeks (c, d). The material was mixed with (a, c) blood and (b, d) blood plasma. [labels: 3 - replacement of the material with new bone tissue, 4 - a young bone, 5 - cement lines, 6 - blood vessel, 8 - Haversian canals, 10 - osteogenesis, 12 - collagen fibers, 13 - mature calcified bone]

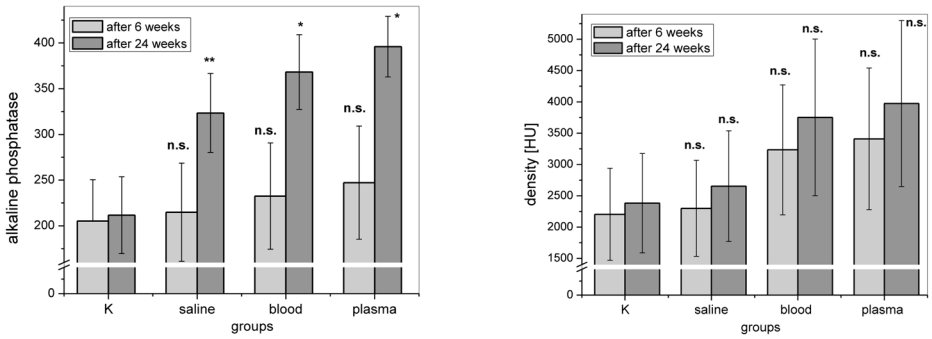

Fig. 9.

(a) ALP content (U/L) and (b) densities of alveolar bone expressed in Haunsfiled units (HU) for the control (K) and experimental groups involving the implantation of HAp/Co2 mixed with saline, blood and blood plasma, 6 and 24 weeks after the implantation. Data are shown as means with error bars representing standard deviation (* => $p < 0.01$ with respect to the control group; ** => $p < 0.05$ with respect to the control group; n.s. => non-significant with respect to the control group).